Source dynamics of radiocesium-contaminated particulate matter deposited in an agricultural water reservoir after the Fukushima nuclear accident

Sylvain Huon, Seiji Hayashi, J. Patrick Laceby, Hideki Tsuji, Yuichi Onda, O. Evrard

Source dynamics of radiocesium-contaminated particulate matter deposited in an agricultural water reservoir after the Fukushima nuclear accident

Sylvain Huon [a,*], Seiji Hayashi [b], J. Patrick Laceby [c], Hideki Tsuji [b], Yuichi Onda [d], Olivier Evrard [c]

[a] Sorbonne Universités UPMC Univ Paris 06, Institut d'Ecologie et des Sciences de l'environnement de Paris (iEES), case 120, 4 place Jussieu, 75 252 Paris cedex 05, France
[b] National Institute for Environmental Science, Fukushima Branch, 10-2 Fukasaku, Miharu, Tamura, Fukushima 963-7700, Japan
[c] Laboratoire des Sciences du Climat et de l'Environnement (LSCE/IPSL), UMR 8212 (CEA/CNRS/UVSQ), Université Paris-Saclay, Centre de Recherche du CNRS - Bât. 12 - Avenue de la terrasse, 91 198 Gif-sur-Yvette, France
[d] Center for Research in Isotopes and Environmental Dynamics, University of Tsukuba, Tennodai, Tsukuba, Ibaraki 305-8572, Japan

HIGHLIGHTS

- FDNPP accident deposited radiocesium over rural-agricultural landscapes in Japan.
- Sources of contaminated particulate matter are examined in Mano Dam reservoir.
- Prominent radiocesium peaks were observed in three out of the four sediment cores.
- Radiocesium and carbon/nitrogen parameters varied between cores and with depth.
- Cultivated sources supplied 48% of particulate matter, subsoil 27% and forests 25%.

GRAPHICAL ABSTRACT

Sources of ^{137}Cs contaminated sediments
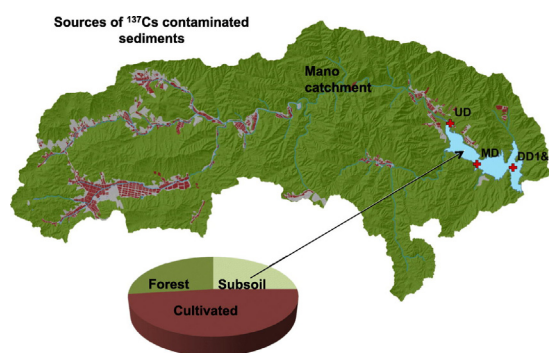
ABSTRACT

The Fukushima nuclear accident in Japan resulted in the deposition of radiocesium over forested and rural landscapes northwest of the power plant. Although there have been several investigations into the dynamics of contaminated river sediment, less attention has been paid to the sources of deposited particulate matter in dams and reservoirs. In the Fukushima Prefecture, there are 10 significant dams and over a 1000 reservoirs for both agricultural and surface water management. These reservoirs may have trapped a significant volume of radiocesium-contaminated sediment. Therefore, characterizing the sources of contaminated particulate matter is important for the ongoing management of contamination in the region.

Accordingly, the composition of particulate matter deposited in the Mano Dam reservoir, approximately 40 km northwest of the power plant, was investigated with the analyses and modelling of carbon and nitrogen stable isotope ratios (δ^{13}C and δ^{15}N), total organic carbon (TOC) and total nitrogen (TN) concentrations. Four sediment cores, with lengths ranging 29–41 cm, were sampled in the Mano Dam. Source samples from 46 forest soils, 28 cultivated soils and 25 subsoils were used to determine the source contributions of particulate matter. Carbon and nitrogen parameters were analyzed on all samples and a concentration-dependent distribution modelling approach was used to apportion source contributions.

Three of the four cores sampled in the Mano Dam reservoir had distinct radiocesium peaks representative of the initial post-accident wash-off phase. Cultivated sources were responsible for 48 ± 7% of the deposited fine

* Corresponding author.
  E-mail address: sylvain.huon@upmc.fr (S. Huon).

particulate matter whereas forests were modelled to contribute 27 ± 6% and subsoil sources 25 ± 4%. Ongoing decontamination of cultivated sources in the Fukushima region should result in a decrease of contaminated matter deposition in reservoirs.

1. Introduction

The Fukushima Dai-ichi Nuclear Power plant (FDNPP) nuclear accident in March 2011 resulted in the fallout of radiocesium over forested and rural landscapes northwest of the power plant. Radiocesium is rapidly bound to fine particles after deposition on the soil surface (He and Walling, 1996; Saito et al., 2014). Thereafter, detachment and transport processes transfer radiocesium contaminated particles downslope and downstream (for a review, see: Evrard et al., 2015). Migration of contaminated particles is accelerated by rice paddy fields that are directly connected to the river network with irrigation systems (Chartin et al., 2013). Accordingly, paddy fields were suggested to be a significant source of particle-bound radiocesium to river systems in the region contaminated by fallout from the FDNPP accident (Lepage et al., 2015; Yoshimura et al., 2016).

Although there have been several investigations into the dynamics of contaminated river sediment (Nagao et al., 2013; Ueda et al., 2013; Yamashiki et al., 2014; Sakaguchi et al., 2015), much less attention has been paid to the sources of deposited particulate matter in dams and reservoirs (Yoshimura et al., 2014). In the Fukushima Prefecture, there are > 10 dams that facilitate agricultural and surface water management and over a 1000 reservoirs (Yamada et al., 2015). These reservoirs may have trapped important volumes of radiocesium-contaminated sediment. For example, the Ogaki Dam on the Ukedo River has been reported to trap 100% of the sand, 95% of the silt and 30–50% of the clay particle size fractions and their bound radiocesium (Kurikami et al., 2014; Yamada et al., 2015). Similarly, a layer of radiocesium contaminated sediment was deposited behind the Yokokawa Dam in the Ota catchment (Chartin et al., 2013).

One approach to investigate the source of this contaminated particulate matter is to use the composition of organic and mineral matter to trace its origin in the catchment. This sediment fingerprinting technique is based on the fact that different sources produce particulate matter with unique parameters or fingerprints (Walling, 2005; Koiter et al., 2013; Owens et al., 2016). Tracing particulate matter back to its potential sources with a fingerprinting technique provides a field-based approach to investigating source dynamics of particulate matter deposited in riverine and lacustrine environments. Particulate matter parameters such as major and trace element geochemistry, mineral magnetic parameters, fallout radionuclide activities and colour have all been used to investigate the contribution of different sources of particulate matter (Grimshaw and Lewin, 1980; Walling and Kane, 1984; Caitcheon, 1993; Murray et al., 1993; Martinez-Carreras et al., 2010; Legout et al., 2013).

In this current research, the origin of contaminated particulate matter deposited in the Mano Dam reservoir, Japan, is investigated with the analysis and modelling of carbon and nitrogen stable isotope ratios (δ^{13}C and δ^{15}N), total organic carbon (TOC) and total nitrogen (TN) concentrations. These bulk organic matter composition parameters have been effectively incorporated into investigations of source contributions to suspended and deposited sediments in various environments (McConnachie and Petticrew, 2006; Fox and Papanicolaou, 2007; Gourdin et al., 2015; Laceby et al., 2015; Laceby et al., 2016). In soils, δ^{13}C broadly discriminates between particulate matter derived from landscapes covered with C_4 vegetation (e.g. several crop and grass species in tropical climates) relative to C_3 vegetation (e.g. tree and temperate grass species) (Schimel, 1993; Mariotti and Peterschmitt, 1994; Fry, 2006). Soil TOC and TN tend to decrease with depth in the soil profile (Blake et al., 2006; Owens et al., 2006), whereas soil δ^{15}N and δ^{13}C

increase (Natelhoffer and Fry, 1988; Amundson et al., 2003). Cultivation of soils, and the related soil organic matter mineralization, is known to reduce TOC and TN contents, resulting in intermediate concentrations relative to surface soils and subsoils (Walling and Woodward, 1995; Juracek and Ziegler, 2009).

Tracing the sources of sediments at the catchment scale with bulk organic matter composition is based on the assumption that, during soil erosion and sediment transport, the breakdown of soil aggregates into fine mineral bound organic matter (Remusat et al., 2012), particulate mineral matter and uncomplexed particulate organic matter (i.e., vegetation debris) should supply sediments that can be labelled by their source compositions (Huon et al., 2006; Hilton et al., 2010; Smith et al., 2013; Laceby et al., 2016). However, the heterogeneous distribution of suspended sediments by water flow (i.e., particle size sorting in rivers) also affects their organic and mineral composition and must be taken into account when investigating sediment deposits (Chaplot and Poesen, 2012; Boix-Fayos et al., 2015; Laceby et al., 2017). In addition, particulate matter in lake sediments does not only originate from soil erosion in the catchment. It also includes sinking debris of decaying autochthonous lake biomass that can be partly preserved in rapidly accumulating deposits (e.g., Thothong et al., 2011). However, in lakes with low productivity, autochthonous inputs are rapidly degraded in the water column (i.e., Sobek et al., 2009). According to Wetzel (2001) < 15% of these inputs reach lake bottom in deep water columns.

In this study, bulk organic matter compositional parameters were used to characterize and quantify the contribution of allochthonous sources (i.e. cultivated soils, forests and subsoils) to particulate matter sampled in four sediment cores collected from the Mano Dam reservoir in the Fukushima region. Determining the source of contaminated particulate matter in water reservoirs (Kurikami et al., 2013; Mouri et al., 2014; Yamada et al., 2015) is an important issue for managing the potential downstream delivery of radiocesium and also provides new insights into its dynamics in lacustrine environments.

2. Material and methods

2.1. Study site

The Mano Dam is located in a mountainous headwater catchment (81 km²), approximately 40 km northwest of the FDNPP. Total radiocesium (^{134}Cs + ^{137}Cs) soil inventories range from ca. 10 to 50 kBq kg^{-1} (Chartin et al., 2013) (Fig. 1). Catchment elevation varies from 170 to 700 m above sea level. The mean annual temperature in the Fukushima region is 11.3 ± 1.7 °C (standard deviation), ranging between 0.0 °C and 23.4 °C for January and August, respectively. The mean annual rainfall is 1420 mm y^{-1} for the fallout impacted area (i.e., 100 km from the FDNPP, Laceby et al., 2016). Importantly, heavy rainfall from tropical cyclones (mainly between July and October) was reported to be a significant factor driving the downstream migration of radiocesium contamination in the region (Evrard et al., 2014; Evrard et al., 2015; Chartin et al., 2017).

Land use for the catchment, classified with a 1-m DEM and satellite imagery from Google Earth (version 7.1.5.1557) is approximately 89% forest, 6% rural residential and 3% cultivated lands. The majority of cultivated land is comprised of paddy fields with irrigation networks that may be connected directly to the river network. The main lithology of the catchment consists primarily of volcanic (40%), granitic (30%), granodioritic (17%), and sedimentary rocks (8%) (GSJ, 2010). The main
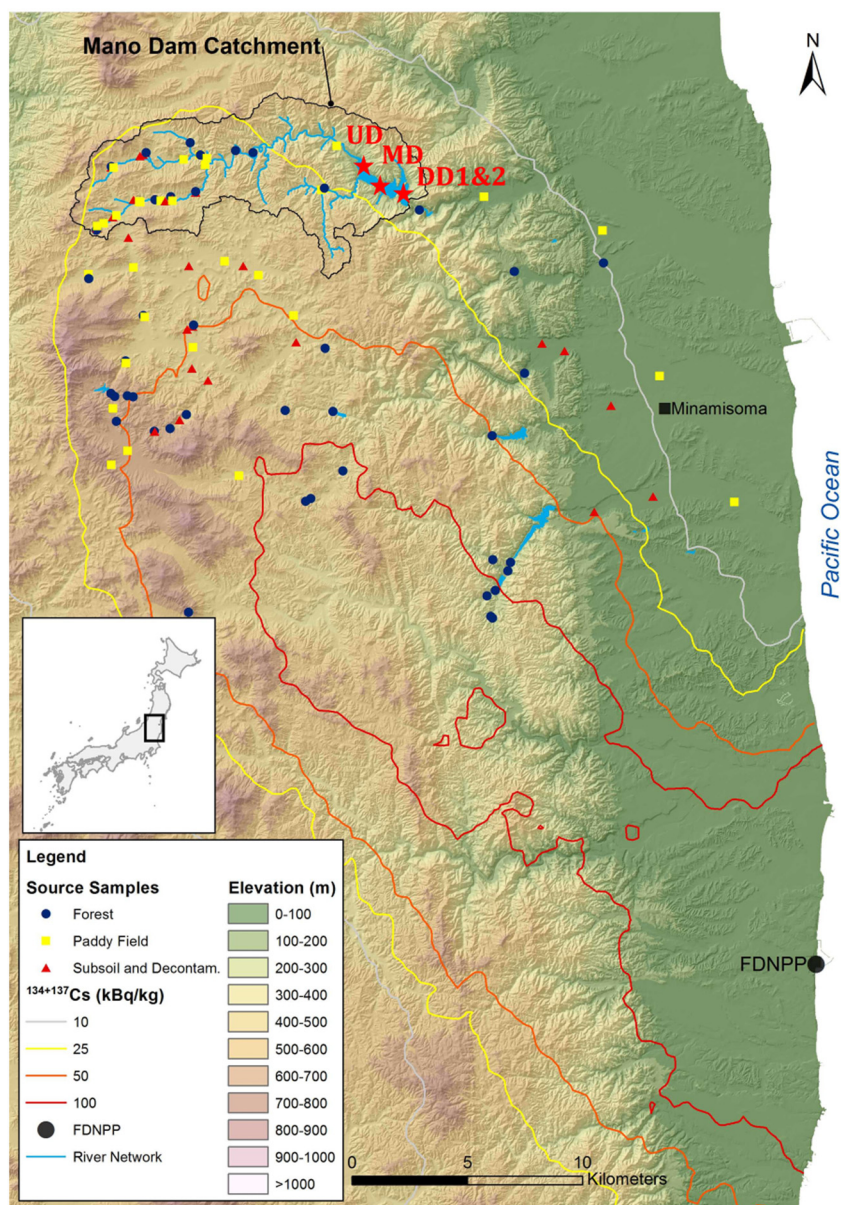
Fig. 1. Mano Dam catchment and location relative to the FDNPP (Fukushima Dai-ichi Nuclear Power plant) including elevation and fallout radiocesium activities from Chartin et al. (2013) with location of the source samples in the region and of the sediment cores UD, MD and DD1 & 2 in lake Hayama (see also details in the graphical abstract).

soils overlaying this lithology are Cambisols (71%), Andosols (20%), Leptosols (3%), and Gley Fluvisols (3%) (NLA, 1972; UNESCO, 1974).

The Mano Dam is the largest reservoir in the region impacted by significant radioactive fallout (e.g. >25 kBq kg^{-1}). It was impounded in 1991, creating lake Hayama, a water body fed by three main tributaries designed for flood control and irrigation, covering 1.75 km^2 with a maximum storage capacity of 36.2×10^6 m^3 and a maximum water depth of 60 m. Discharge into the Mano Dam covering the period 2007–2015 (Supplementary information Fig. 1, Fukushima Prefecture Data) may exceed 100 m^3 s^{-1} during major flow events. Total suspended solids have reached 1 g L^{-1} (Hayashi, unpublished data). During summer and fall in 2014 and 2015, water temperature ranged from 9 to 25 °C near the surface and 6–16 °C at 20–50 m water depth. Lake biological production was rather limited as shown by low chlorophyll-a pigment concentrations (1.0–3.6 μg L^{-1}) measured in the superficial 0.5 m water layer during the same period (Hayashi, unpublished data). Suboxic to anoxic conditions prevailed in the bottom layer of the deep-water columns, below 46–50 m water depths. Given the dominance of a forest cover in its drainage area (89%), lake Hayama is very

likely oligotrophic and hosts little aquatic vegetation, as discussed by Knoll et al. (2015) in their study of linkages between reservoir eutrophication and landscape characteristics. In addition, the water residence time of ca. 0.48 years (Fukushima and Arai, 2014; Matsuda et al., 2015) and the location within a coastal mountainous region induce high sediment accumulation, in particular after heavy rainfall and typhoon events (Evrard et al., 2016; Laceby et al., 2016; Lepage et al., 2016).

2.2. Field sampling

Four sediment cores with a diameter of 11 cm were sampled in lake Hayama. No seasonal alternation of lake biomass and terrigenous sediment layers was visible (Supplementary information Fig. 2). The upstream dam core (UD) was sampled 3.5 m below the water surface, the midstream dam core (MD) was sampled at 18 m depth, and two downstream dam cores (DD1 and DD2) were sampled at 45 m water depth. On November 22, 2014, divers recovered the UD and MD cores using hand-held piston corers. The DD cores were sampled with a gravity-based corer (HR type, RIGO, Tokyo, Japan) within 20 m of each other

on April 24, 2015. The length of the sediment cores ranged between 29 cm (DD2) and 41 cm (MD).

Source soil samples were obtained from the three main sources in the region that were selected after stakeholder consultations, multiple fieldwork campaigns and a literature review (Evrard et al., 2015). In total, 46 forest (16 coniferous, 15 deciduous, and 15 mixed), 28 cultivated (14 rice paddy and 14 other fields), and 25 subsoil samples (15 decontaminated soil and 10 channel bank and subsoil erosion scars) were collected in the region based primarily on pragmatic factors, such as road and property access (Laceby et al., 2016) (Fig. 1). Decontamination of soils involves the removal of surface vegetation and the replacement of the topsoil layer (ca. 5 cm) with a new substrate, made of crushed gravel with similar properties than subsoils. Later phases of decontamination will introduce a new topsoil layer, although this phase was not implemented in the Mano Dam catchment during the sampling period.

To sample surface sources, a small plastic trowel was used to combine 10 surface scrape subsamples (top 1–2 cm, approximately 5 g) into one sample. The decontaminated soils were sampled with the same method used for surface soils. Subsoils were sampled by first removing the exposed sidewall of channel banks and hillslope erosion features and then the exposed subsoil was sampled with 10 plastic trowel grabs that were combined into one sample.

2.3. Sample processing and analyses

Upon returning from the field, the cores were sectioned into 1 cm increments from 0 to 15 cm depth, in 2 cm intervals from 15 to 25 cm, and in 3 cm increments until the base of the cores as the objective was to investigate the distribution of radiocesium in the cores. Sectioned subsamples were oven-dried (60 °C) at the National Institute of Environmental Studies (NIES), Japan, where they also underwent gamma spectrometry analyses with coaxial high-purity germanium detectors SEG-EMS GEM 20–70 (efficiency: 23%) and GEM 35–70 (efficiency: 40%) (Seiko EG&G Co. Ltd., Tokyo, Japan), using Gammastudio (Seiko EG&G Co. Ltd., Tokyo, Japan) analyzing software. As a standard radioisotope source, MX033U8PP (The Japan Radioisotope Association, Tokyo, Japan) was used for efficiency calibration. Measured radioactivity of ^{137}Cs was decay-corrected to the sampling date and uncertainty of ^{137}Cs measurements was 4% for both detectors.

Particle size analyses were performed for each subsection of the cores with a laser diffraction particle size analyzer (SALD-3100, SHIMAZU, Kyoto, Japan) at NIES without ultrasonic dispersion and adjusting the suspended concentration to ca. 100 mg L^{-1}. As water flow velocity decreased in the lake, fine-sized particles are preferentially transported downstream. Therefore, for organic matter analyses, all samples were sieved to <63 μm to remove small stones and coarse vegetation debris, and to avoid sorting effects when comparing sediment cores recovered at different distances from the main inlets. Samples were first dry-sieved to <2 mm and thoroughly homogenized. Thereafter, subsamples were wet-sieved to <63 μm with deionized water. The <63 μm fractions were finely ground and homogenized with an agate mortar, weighed, and packed for analyses into tin capsules. Forty percent of the samples were randomly selected and treated with a 10% HCl solution to test for the presence of carbonate minerals. As there was no CO_2 bubbling in any of the samples, which would reflect dissolution of carbonate minerals, it was concluded that the carbon associated with particulate matter was organic in nature (Gourdin et al., 2015). X-Ray powder diffraction patterns of selected samples were also performed to control the possible occurrence of carbonate minerals (e.g. Brindley and Brown, 1982). The major diffraction peaks, typical for the most common minerals, calcite at 3.035 Å (104), aragonite at 3.39 Å (111) and 3.27 Å (021) and dolomite at 2.888 Å (104), were not detected at the 2% uncertainty level. Therefore, no treatment for carbonate removal was performed.

A continuous flow Elementar® VarioPyro cube analyzer coupled to a Micromass® Isoprime Isotope Ratio Mass Spectrometer (EA-IRMS) at the Institute of Ecology and Environmental Science (iEES) in Paris was used for all total organic carbon (TOC) and total nitrogen (TN) elemental and isotopic (δ^{13}C and δ^{15}N) analyses. First, TOC and δ^{13}C were measured for all <63 μm fractions together with a set of tyrosine standards (Coplen et al., 1983). A second analysis run was conducted on aliquots of the same samples after weight optimization for TN and δ^{15}N. Oxygen for combustion was injected during 70 s (30 mL min^{-1}) and temperatures were set at 850 °C and 1120 °C for the reduction and combustion furnaces, respectively (Agnihotri et al., 2014). Analytical precision was determined with the repeated analyses of a tyrosine standard ($n =$ 56), calibrated against international reference standards (Girardin and Mariotti, 1991). Mean uncertainties were 0.2% for TN, 0.1% for TOC, 0.1‰ for δ^{13}C (vs. PBD) and 0.2‰ for δ^{15}N (vs. Air). All sediment core data are reported in the supplementary information (Table S1) and the source dataset is published in Laceby et al. (2016).

## 2.4. Statistical analyses and source modelling

Prior to modelling source contributions, ^{137}Cs activities were examined in the bulk sediment samples. This analysis focuses on ^{137}Cs ($t_{1/2}$ ca. 30 years) as the shorter half-life of ^{134}Cs ($t_{1/2}$ ca. 2 years) has resulted in ca. 87% depletion of the original fallout in this environment by March 2017 (i.e., 6 years after the accident) compared to only a ca. 13% depletion for ^{137}Cs during this period. After radiocesium activity determinations, TOC, TN, δ^{13}C and δ^{15}N were measured in each core on the <63 μm fractions. All parameters were also plotted together with the source data set for this particle size fraction (Fig. 2).

Models were then run to quantify particulate matter source contributions to the core material with three different parameter property combinations: 1) TN and δ^{15}N (the N model); 2) TOC and δ^{13}C (the C model); 3) all 4 properties (the C + N model). These combinations were used to incorporate potential differences between modelling carbon and nitrogen separately into an overall model uncertainty estimation. The source contributions to particulate matter in the sediment cores were modelled for these three different parameter groupings with a concentration-weighted distribution modelling approach (Laceby et al., 2015; Le Gall et al., 2016).

Where C_i is the TOC or TN concentration in the sediment core particulate matter, S_{si} is the TOC or TN (i) concentration in source (s), C_r is the carbon or nitrogen stable isotope ratio (r) in particulate matter, S_{sr} is the carbon or nitrogen stable isotope ratio (r) in source (s), W_{si} is the TOC or TN concentration in source (s) that is used to weight the respective carbon or nitrogen isotopic ratio (r), x_s is the relative contribution of source (s); and MMD is the mixing model difference that is minimized when summing absolute values and solving Eq. (1).

$$
\begin{aligned}
\mathrm{MMD} = \mathrm{ABS}\ & \left(C_i - \left(\sum_{s=1}^{m} S_{si} x_s \right) \right)/C_i \\
& + \mathrm{ABS}\ \left(C_r - \left(\left(\sum_{s=1}^{m} S_{sr} W_s x_s \right) \middle/ \sum_{s=1}^{m} W_s x_s \right) \right)/C_r
\end{aligned}
\tag{1}
$$

Non-negative constraints were imposed on elemental concentrations and Pearson product-moment correlation coefficients incorporated within-source correlations between source parameters during the modelling process (Laceby and Olley, 2015). Distributions were fit to source parameters with Oracle's Crystal Ball Software following the approach of Laceby et al. (2016). For core parameter distributions, normal distributions were fit around individual core sample parameters by substituting analytical uncertainty for the parameter standard deviation similarly to Wilkinson et al. (2015) and Evrard et al. (2016). The model was run with the Optquest algorithm in Oracle's Crystal Ball Software (Haddadchi et al., 2014; Foucher et al., 2015; Laceby and Olley, 2015).
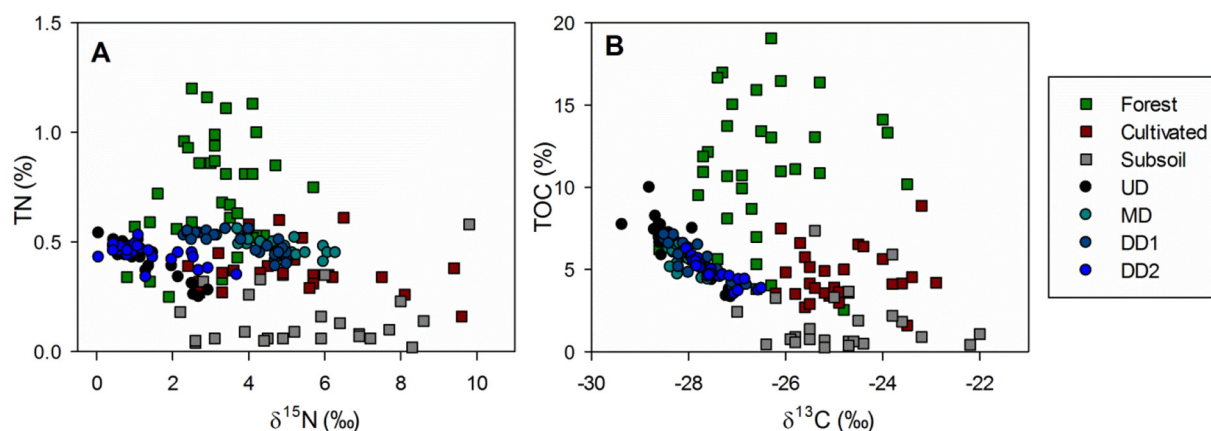
Fig. 2. Plot of particulate matter parameters with : A) $\delta^{15}N$ vs. TN and B) $\delta^{13}C$ vs. TOC for all sediment core samples (UD, MD, DD1 and DD2) together with soil source samples (Forest, Cultivated and Subsoil from Laceby et al., 2016).

With the Optquest algorithm, the mean and standard deviation for each source's contribution distribution (x_s in Eq. (1)) were simulated along with all other parameters, solving the model equation 2500 times for each core sample distribution. For these simulations, 2500 random samples (Latin Hypercube – 500 bins) were drawn from each distribution with the objective to minimize the MMD with the different source contributions. This model solving process was then repeated 2500 times, to reduce the standard error in the model and provide an additional term for model uncertainty, with the median relative source contribution (x_s) from these 2500 additional simulations used as individual source contributions.

Model run uncertainty was determined by summing the standard deviation of the individual source contribution with the median absolute deviation (MAD) of these contributions, and the MAD of all the modelled standard deviation for the additional 2500 model simulations (Laceby et al., 2015). The mean differences between the different model runs (i.e. C Model, N Model and C + N Models) were added to their individual uncertainties to provide a cumulative model error that incorporates both the model uncertainty and the differences between the model runs. Sigmaplot (v. 12.5) was used for plotting data and for statistical analyses except for the Pearson product-moment correlation coefficients, which were conducted in Microsoft Excel with the analysis took-pack add-in.

3. Results

3.1. Radiocesium activities and sediment grain size

Prominent radiocesium peaks were evident in the MD, DD1 and DD2 cores though not in the UD core (Fig. 3). For the latter, ^{137}Cs activities started to increase at a sediment depth of 13 cm and gradually increased to a peak concentration of 12 kBq kg^{-1} at the top of the core. In the MD core, ^{137}Cs activities started increasing above 15 cm sediment depth, and peaked at 54 kBq kg^{-1} at 10 to 11 cm (dashed line in Fig. 3). Thereafter, the ^{137}Cs activities in the MD core declined to a mean of 28 ± 2.1 kBq kg^{-1} in the top 9 cm of the core. For the DD1 core, ^{137}Cs activities also started to increase at a depth of 17 cm and peaked at 40 kBq kg^{-1} at 11 to 12 cm before declining to a mean of 17 ± 2.1 kBq kg^{-1} in the top 8 cm of this core. For the DD2 core, ^{137}Cs activities started to increase at a depth of 15 cm and peaked at 50 kBq kg^{-1} at 8 to 9 cm before declining to a mean of 24 ± 2.0 kBq kg^{-1} in the top 5 cm of the core. For the MD and DD cores, ^{137}Cs activities were reduced by 47 ± 4% in the upper sections of these cores.

Particle size distributions also varied in the different cores. The mean D_{50} of the UD core (63 µm) was greater than that of the other three cores

(MD: 16 µm, DD1: 31 µm, DD2: 24 µm). The D_{50} of the MD and DD2 cores were the most stable with standard deviations of 3.3 µm and 3.8 µm, respectively, whereas the DD1 and UD cores were more variable in their depth profiles with 10 µm and 31 µm, respectively. The maximum D_{50} in the DD1 core was 57 µm compared to 138 µm in the UD core.

3.2. TOC and TN parameters in the sediment cores

Carbon and nitrogen parameters in the sediment cores also varied. TOC ranged from a mean (±1 standard deviation) of 6.5 ± 1.6% in the UD core to 4.9 ± 0.7% in the MD core with DD1 (5.8 ± 1.0%) and DD2 (5.6 ± 0.8%) plotting in between. Both DD cores display decreases in TOC during the ^{137}Cs peak. There was no major discernible peak in the MD core and the UD core had a peak near 10% TOC at ca. 13 cm depth. This peak was followed by a decline to ca. 3% around 25–30 cm depth before increasing to ca. 5% at the base of the core. The UD core had the most pronounced variations, with TOC content gradually declining with sediment depth in the other three cores. There was less variation in TN content between the different sediment cores with mean TN (±1 standard deviation) in these cores ranging from 0.49 ± 0.04% in DD2 and 0.49 ± 0.05% in DD1 to 0.42 ± 0.08% in the UD core, with the MD core plotting in between (0.45 ± 0.04%). The TN concentration trends generally reflected TOC variations with declines in TN during the ^{137}Cs peak for DD1 and DD2. The exception is the TOC peak in the UD core that had no equivalent for TN.

Contrasts between the UD core and the other three cores were particularly clear for the TOC/TN ratio. Mean values (±1 standard deviation) for the UD core were 15.3 ± 1.2 compared to 11.0 ± 1.1 for the MD core, 11.3 ± 0.9 for the DD2 core, and 11.7 ± 1.0 for the DD1 core. The high TOC/TN ratio of the UD core is likely indicative of higher abundances of uncomplexed organic matter such as leaf litter and vegetation debris, relative to the other three sediment cores, that are characterized by fine-grained soil organo-mineral complexes with low TOC/TN ratios close to 10 to 12 (the grey shaded area in Fig. 3). When examining TOC and TN more closely (Fig. 4), sediments collected in the shallow environment of core UD plot separately from the others sampled at deeper water sites. Both parameters are correlated and, for such a relationship, the zero-intercept value of the correlation line reveals the magnitude of possible inorganic nitrogen excess (Schubert and Calvert, 2001; Nieder et al., 2011). The zero intercept is lower in core UD (0.10 ± 0.01, $r = 0.98$) than for the other three cores (0.17 ± 0.01, $r = 0.93$), highlighting a composition, more organic in nature and with a lower clay-bound ammonium content that characterize cultivated soils. When considering both D_{50} and the TOC/TN ratio, the
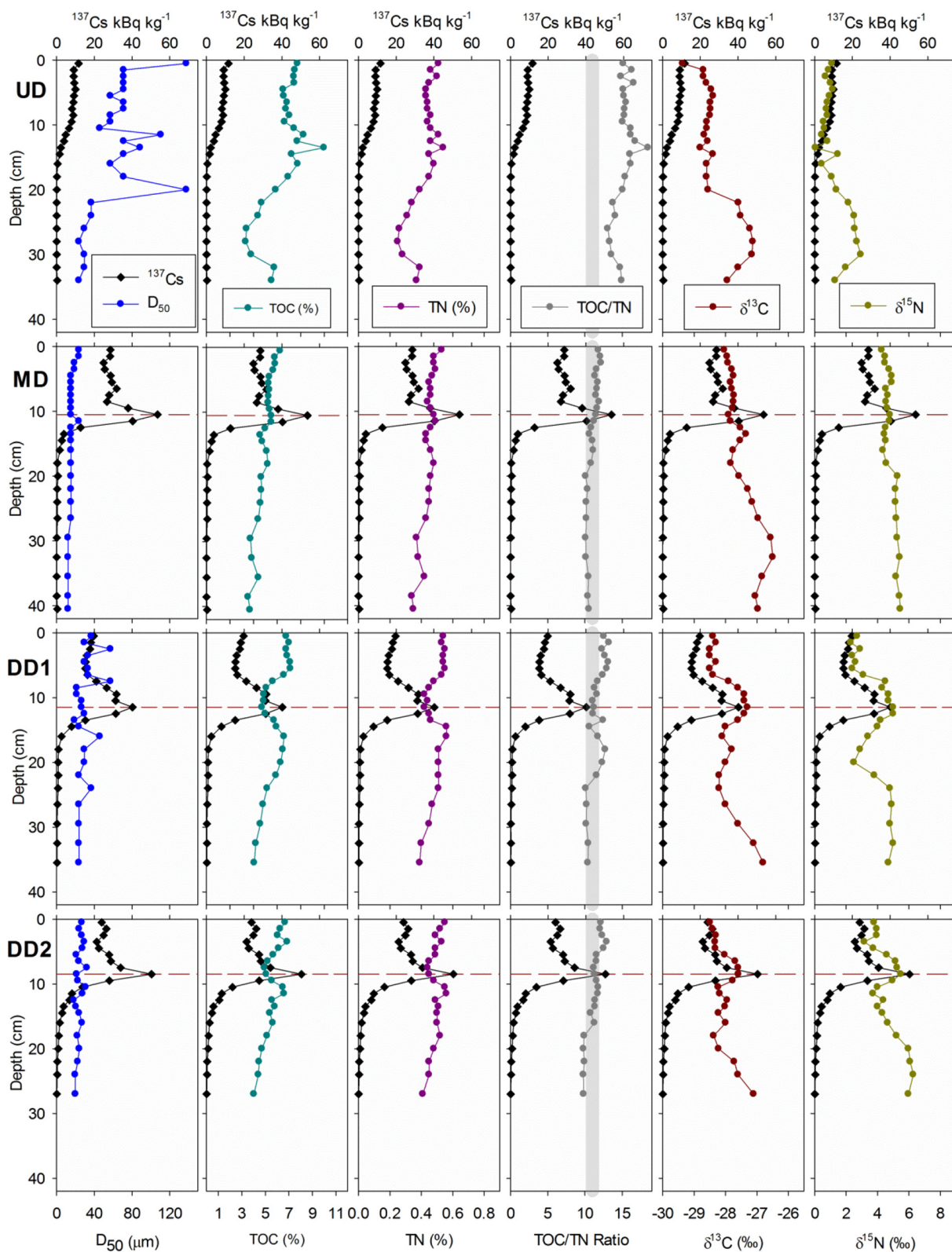
Fig. 3. Plots of sediment core variation in ¹³⁷Cs activity (top horizontal axis) compared to the different parameters discussed in the text (bottom horizontal axis). The dashed red line indicates the location of the prominent ¹³⁷Cs peaks and the shaded area represents the TOC:TN ratio between 10 and 12 typical for soil organic matter. (For interpretation of the references to colour in this figure legend, the reader is referred to the web version of this article.)

sediments in the UD core are comprised of coarser particulate matter and it is difficult to quantify their sources with mixing models targeting the <63 μm size fraction.

Each of the four cores had similar mean $\delta^{13}C$ values (± 1 standard deviation), ranging from -28.3 ± 0.6‰ in the UD core to -27.5 ± 0.5‰ in the MD core, with the DD1 core (-27.9 ± 0.5‰) and the
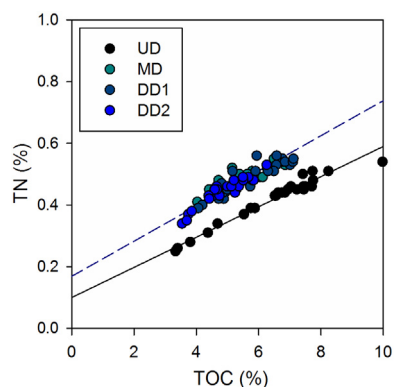
Fig. 4. Plot of TOC vs. TN concentrations for all sediment cores with correlation lines. The plain line fits UD sediment samples and the dash line fits DD1, DD2 and MD sediment samples.

DD2 core (-28.0 ± 0.4‰) plotting in between. In contrast to TOC and TN, $\delta^{13}C$ increased with the ^{137}Cs peaks in the DD1 and DD2 cores. The MD core did not have a $\delta^{13}C$ response corresponding to the ^{137}Cs peak, although there was an increase below this peak. There was no immediate change in the UD core $\delta^{13}C$ during the ^{137}Cs deposition period, although a sharp increase can be observed in the lower sections of this core. In all four cores, $\delta^{13}C$ increased with depth by a mean of 1.4 ± 0.2‰ from the top to the base of these cores.

Relative to $\delta^{13}C$, there were greater differences between the individual cores for $\delta^{15}N$. Mean $\delta^{15}N$ (± 1 standard deviation) ranged from 1.2 ± 0.8‰ in the UD core to 4.8 ± 0.4‰ in the MD core. The two DD cores plotted closer to the MD core with a mean of 4.7 ± 0.9‰ in the DD2 core and 3.8 ± 1.0‰ in the DD1 core. The $\delta^{15}N$ trend in the depth profiles generally follows that of $\delta^{13}C$ with increases with the ^{137}Cs peak in the two DD cores and a mean gradual increase (1.4 ± 0.9‰) in the four cores. The main difference compared to $\delta^{13}C$ was that the increase with depth was greater in the two DD cores (2.1 ± 0.4‰) compared to the UD core (0.2‰). Furthermore, there were very limited variations

in $\delta^{15}N$ throughout the MD depth profile. Of note, the $\delta^{13}C$ and $\delta^{15}N$ of particulate matter at the ^{137}Cs peak level are similar to those at the base of the two DD cores. Cumulatively, the TOC, TN and the isotope values appear to be more responsive to the ^{137}Cs deposition (e.g. peak ^{137}Cs) in the two DD cores whereas the MD core has constant parameters throughout the depth profile, and the UD core has a distinct trend indicative of a different source composition.

3.3. Source soil contribution to particulate matter

Bulk organic matter composition parameters provided significant discrimination between the three main sources (Fig. 5). In particular, all tracer parameters provided significant discrimination between forest and cultivated sources, and also between forest and subsoil sources (Supplementary information Table S2). Only TOC and TN provided significant discrimination between cultivated and subsoil sources. Relative to sediment sources, particulate matter TN plots generally between forest and cultivated source samples whereas $\delta^{15}N$ plots similarly close to the paddy fields, though increasingly closer to the subsoil sources (Fig. 2A). Particulate matter TOC plots similarly to TN, between paddy fields and forest sources. Core $\delta^{13}C$ plots from the lower end of the forest sample range (e.g. UD) towards the cultivated and subsoil sources (e.g. MD and DD2) (Fig. 2B). With the exception of some UD samples, core samples all plot within the potential source range, allowing for the core particulate matter to be modelled with the source dataset.

Quickly it becomes evident that there was larger cumulative modelling uncertainty for the UD core ($24 \pm 3\%$) compared to the other three cores ($10 \pm 3\%$) (Fig. 6). The higher D_{50} and TOC/TN ratios indicate that the UD core is comprised of coarser particulate matter, resulting in these elevated model uncertainties. Accordingly, no cumulative source contributions from this core will be included in the overall model results. For the other three cores, cultivated sources were the dominant source of particulate matter, contributing $48 \pm 7\%$ of particulate matter, followed by forest sources ($27 \pm 6\%$) and subsoil sources ($25 \pm 4\%$).

Forest source contributions were clearly lower during the ^{137}Cs concentration peak in both DD cores though this was not evident in the MD core, where subsoil source contributions decreased during the ^{137}Cs
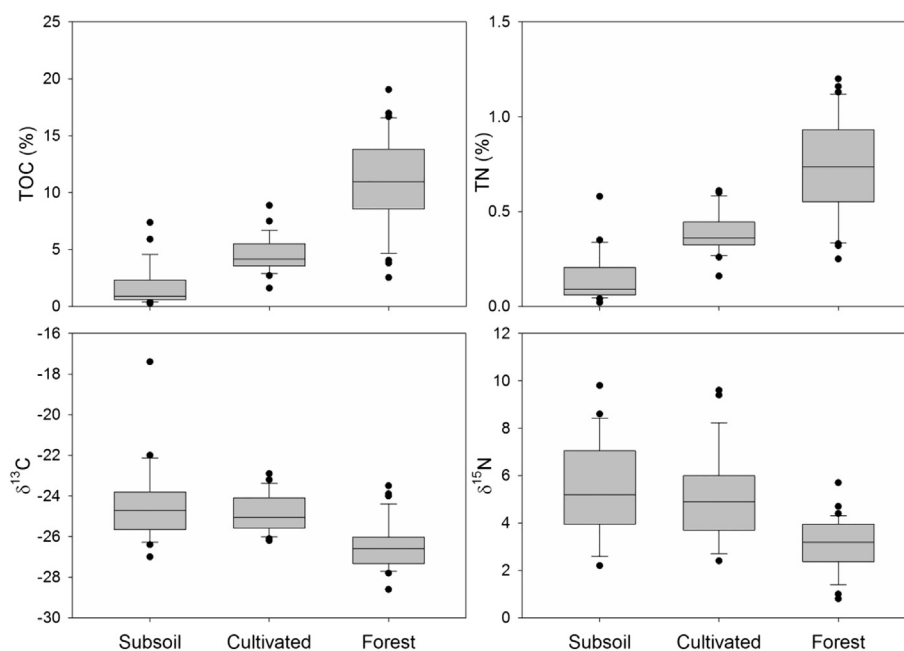
Fig. 5. Box plots of each of the particulate matter parameters in the different soil sources of sediments (data in Laceby et al., 2016).
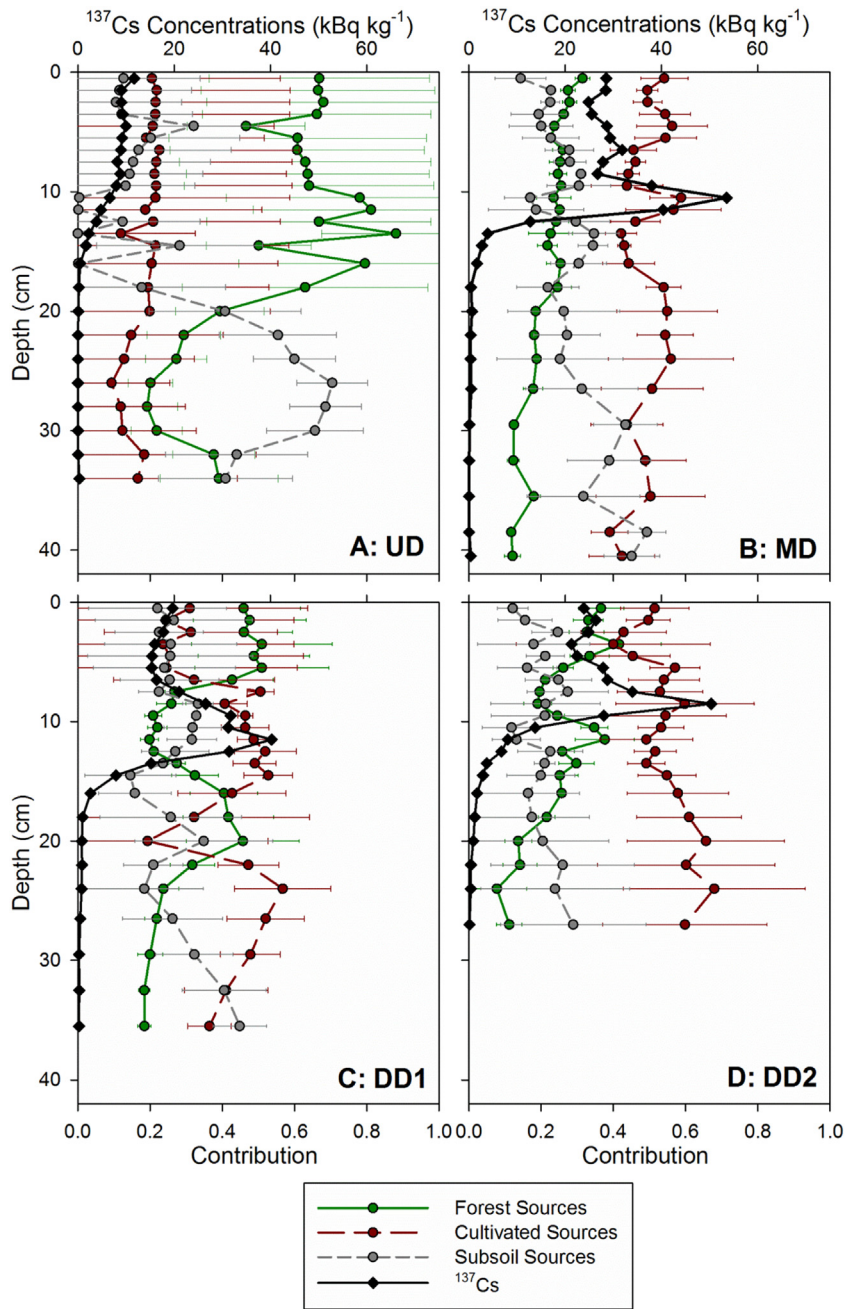
Fig. 6. Plots of ^{137}Cs activities (diamonds) of modelling results (circles with different dashed lines) for A) the UD core, B) the MD Core, C) the DD1 Core, and D) the DD2 Core with the error bars indicative of the compiled modelled error as outlined in section 2.4.

peak. Conversely, the subsoil source contribution decreased during the ^{137}Cs peak in the DD1 core with a less obvious impact for the DD2 core. For both the MD and DD1 cores, the contribution of subsoil sources is greatest at the base of the core. Interestingly, forest sources are the main source of particulate matter in the DD1 core whereas cultivated sources are the main source in DD2 core. These variations of source contributions should be considered within their overall uncertainty as most of the above-mentioned variations occur within the source contribution uncertainty. Of note, the model uncertainty is elevated in the sediment cores by adding the individual model uncertainty with the differences obtained with the various iterations modelled (i.e. C Model, N Model, and the C + N Model) to incorporate differences in the input parameters. Ultimately, cultivated sources are the dominant source of particulate matter in the Mano Dam catchment followed by forest and

subsoil sources with these latter two sources contributing sediment in similar proportions.

4. Discussion

4.1. Sources of radiocesium

Three of the cores (MD, DD1, and DD2) exhibited peak ^{137}Cs activities after the accident that quickly receded by ca. 50% in the top sediment layers of the cores reflecting the radiocesium wash-off and migration phase in the Mano catchment following the FDNPP accident. The peak in ^{137}Cs activities is likely be related to two events: Typhoon Songda (May 2011) or Typhoon Roke (September 2011). In particular, Typhoon Roke has been reported to move a significant amount of

contaminated sediment downstream (Nagao et al., 2013; Ueda et al., 2013; Yamashiki et al., 2014). As a rapid decline in radiocesium migration may be expected after a nuclear accident (Garcia-Sanchez, 2008; Garcia-Sanchez and Konoplev, 2009), this initial peak likely reflects initial wash-off and downstream migration of ^{137}Cs during the first six months following the FDNPP accident. Unfortunately, this dataset does not allow for the identification of the typhoon, Songda and/or Roke, responsible for the prominent ^{137}Cs peaks.

4.2. Core parameter variation

A variety of trends were evident in the sediment cores regarding carbon and nitrogen parameters. First, there were clear differences between the UD and the other three cores. The ^{137}Cs depth suggests that particulate matter deposited at the UD core site involved different processes relative to the other three cores. The particle size distributions indicated that the UD sediment is comprised of fine and coarser sand relative to the other cores again suggesting that the UD core is controlled by different sedimentation processes than the other three cores. The elevated TOC/TN ratio in the UD core indicated that it likely contains coarser particulate organic material (e.g. vascular plant roots and litter) relative to the other core samples (MD, DD1 and DD2) characterized by a ratio remaining within the 10–12 range of soil organic matter values. The latter are assumed to correspond to stabilized mineral-bound organic matter as found in a wide range of soils (Hedges and Oades, 1997; Onstad et al., 2000; Kirkby et al., 2011).

Material deposited at the UD site may reflect ongoing, gradual particle-bound radiocesium input in the shallow parts of the reservoir, with local wetlands acting as a buffer to sediment transport (diCenzo and Luk, 1997). This supply possibly accounts for the deposition of ^{137}Cs bound particulate organic matter during low flow periods with total suspended sediment loads lower than 25 mg L^{-1} as reported by Naulier et al. (2017). Combined with the gradual increase in ^{137}Cs activity, the material may also highlight particle size sorting processes, leading to preferential deposition of coarse particulate organic matter and sand near reservoir inlets during storm flow events due to the decrease of stream water velocity when entering the lake. In contrast, fine material (DD and MD cores) settled further downstream in the deep water columns of the reservoir, as reported for other lakes in SE Asia (Thothong et al., 2011).

Aside from the larger variation between the UD and the other cores, there was also variation between MD and the DD cores, and between the two DD cores. The MD core consisted of the finest material with the most consistent TOC/TN ratio throughout the core. Conversely, the two DD cores had higher D_{50} and TOC/TN ratios indicative of a coarser organic material. The MD core was likely sampled at a location where only consistent fine particle matter settles, whereas the two DD cores were influenced by a local tributary, likely the tributary north of their sampling location (Fig. 1). Differences between the D_{50} and TOC/TN ratio in the two DD cores are either related to the influence of material deposition from this local tributary, highlighting the potential heterogeneity in particulate matter deposition in reservoirs.

4.3. Tracing particulate matter sources of sediments with organic matter properties

Due to the low productivity of the lake, inferred from low chlorophyll-a concentration measurements, to the lack of seasonal alternations of lake biomass and terrigenous sediment layers (e.g. Thothong et al., 2011) that would reflect lasting periods of high surface production and to the connection of sediment deposits with major typhoons, soil derived organic matter likely represented the major input to lake sediments. However, solely using δ^{13}C values, it is not possible to discriminate the possible contribution of freshwater phytoplankton (Lehmann et al., 2004; Cailleaud, 2015) from that of soil organic matter (e.g. Mook and Tan, 1991; Lee et al., 2011; Sakai et al., 2013) as their isotopic

signatures may partly overlap. More accurate identification is performed using all the organic matter properties.

Selective degradation of chemical compounds in the water column and in the superficial sediment layer of the Mano Dam reservoir may also have modified the composition of source organic matter (Colombo et al., 1997; Rontani and Volkman, 2003; Giri et al., 2015; Chen et al., 2017). There was, however, no clear evidence of any property degradation trend with sediment depth in the cores, such as decreasing hyperbolic profiles for TOC concentration (e.g. Emerson, 1985). Therefore, bulk identifiers of terrestrial matter sources in Mano Dam reservoir sediments likely underwent limited decomposition (Meyers, 1994), keeping their main carbon properties constant (e.g, Nguyen Tu et al., 2017).

Coupling bulk carbon and nitrogen tracing parameters with other indicators of source dynamics such as biomarkers (Chen et al., 2017) or compound specific stable isotopes (Blake et al., 2012; Reiffarth et al., 2016) should provide additional insight on particulate matter preservation and source dynamics and their potential impact on modelling results. Based on this study, cultivated sources (48 ± 7%) were the dominant source of particulate material in all three lower dam cores (MD, DD1, and DD2) with forests (27 ± 6%) and subsoil sources (25 ± 4%) having similar contributions (Fig. 6). In these three cores, there were increases in the cultivated source contributions along with the peak in ^{137}Cs activities, although this peak was not as distinct as the individual particulate matter parameters as shown in Fig. 3. In the MD and DD1 cores, there were varying cultivated source contributions throughout the core, which may reflect the occurrence of contrasting hydro-sedimentary events. Ultimately, the source contributions to particulate matter sampled in the sediment cores are related to the dynamics of sediment deposition within the reservoir.

These results are different from those obtained for river systems in the main fallout-impacted region (Laceby et al., 2016) that reported subsoils as being the dominant source (45 ± 10%), followed by cultivated (38 ± 19%) and forest sources (17 ± 10%). The increase in cultivated and forest source contributions to reservoir sediments compared to those found in other river sections is likely attributed to particle size sorting effects where the particulate matter traced in the river systems constituted a coarser particle size fraction than what was traced in the deep water column of the Mano Dam reservoir. Preliminary measurements carried out in the framework of the AMORAD project (see further in the acknowledgements) showed that river sediments displayed a higher D_{50} (mean: 100 μm) than sediment cores in the Mano Dam reservoir (16–63 μm, this study). Accordingly, different priorities may be required for managing the deposition of contaminated particulate matter in reservoirs compared to riverine environments.

4.4. Management implications

In the region impacted by fallout from the FDNPP accident, Japanese authorities have made significant progress in the decontamination of rural residential areas and paddy fields (Yasutaka and Naito, 2016). Often, this remediation includes stripping the surface vegetation and also replacing the top ca. 5 cm of the soil with a new contaminant-free substrate. In total, this decontamination has been estimated to cost between 1 and 16 trillion yen (e.g. ca. 10–140 billion USD) for ca. 9000 km^2 (Yasutaka and Naito, 2016). In the context of this current research, the decontamination of rice paddy fields should dramatically reduce the amount of radiocesium available for mobilization, transport and deposition in the region's dams and reservoirs (Evrard et al., 2016). As cultivated sources were modelled to contribute nearly 50% of the material sampled in the Mano Dam, this decontamination has significant potential to reduce downstream radiocesium contamination. This is particularly important as these areas are highly connected to the soil network through irrigation systems. Of note, forest and subsoil sources were modelled to contribute the other half of particulate matter deposited in the reservoir and more research is required to further

characterize the forest source contribution as this material has the potential to be an ongoing source of radiocesium contaminated particulate matter to downstream dams and reservoirs in the region.

The MD and DD cores clearly indicated a significant deposition of radiocesium-contaminated sediment in the Mano Dam reservoir. If the radiocesium in the Mano Dam cores was only derived from direct atmospheric fallout and with a 1:1 activity ratio of $^{137}Cs/^{134}Cs$, we would expect there to be approximately 10 kBq kg^{-1} of ^{137}Cs in total in the top 5 cm of the sediment cores (Fig. 1) (Chartin et al., 2013). When examining Fig. 6, it becomes quickly evident that there is significantly more radiocesium deposited in the Mano Dam that would be expected from atmospheric fallout alone. The accumulation of radiocesium-contaminated sediment in the reservoirs in the region impacted by fallout represents an ongoing management challenge, as there are several large dams with higher activities of ^{137}Cs than the Mano Dam (Fig. 1). Furthermore, there are hundreds of smaller farm dams in the fallout- impacted region, which may be used to irrigate rice paddy fields, that may also have been contaminated by the deposition of ^{137}Cs. Together these water supply reservoirs have potentially trapped significant volumes of sediment-bound ^{137}Cs resulting in potential long-term impacts that will likely require ongoing management and monitoring.

5. Conclusions

Three of the four cores sampled in the Mano Dam reservoir had distinct ^{137}Cs peaks representative of the initial post-accident wash-off phase. The UD core is likely more representative of the processes governing coarse materials (e.g. bed load processes) whereas the other three cores (MD, DD1 and DD2) are representative of the processes governing the downstream transport and deposition of fine soil particles (e.g. <63 μm). The differences in these processes are highlighted by the ^{137}Cs, D_{50}, and TOC/TN ratios of particulate matter in the latter three cores compared to the UD core.

Cultivated, forest and subsoil sources all contributed particulate matter downstream. Cultivated sources were responsible for 48 ± 7% of the deposited fine particulate matter (e.g. MD, DD1, and DD2 cores), whereas forests contributed 27 ± 6% and subsoil sources contributed 25 ± 4%. The decontamination of cultivated sources in the Fukushima region should result in a decrease of contaminated matter deposition in reservoirs. Additional investigations are however required to understand the potential ongoing source contributions from forested landscapes in this post-accidental context.

Supplementary data to this article can be found online at http://dx.doi.org/10.1016/j.scitotenv.2017.07.205.

References

Agnihotri, R., Kumar, R., Prasad, M., Sharma, C., Bhatia, S., Arya, B., 2014. Experimental setup and standardization of a continuous flow stable isotope mass spectrometer for measuring stable isotopes of carbon, nitrogen and sulfur in environmental samples. Mapan 29, 195–205.

Amundson, R., Austin, A.T., Schuur, E.A.G., Yoo, K., Matzek, V., Kendall, C., Uebersax, A., Brenner, D., Baisden, W.T., 2003. Global patterns of the isotopic composition of soil and plant nitrogen. Glob. Biogeochem. Cycles 17, 1031.

Blake, W., Walsh, R., Sayer, A., Bidin, K., 2006. Quantifying fine-sediment sources in primary and selectively logged rainforest catchments using geochemical tracers. Water Air Soil Pollut. Focus 6, 615–623.

Blake, W.H., Ficken, K.J., Taylor, P., Russell, M.A., Walling, D.E., 2012. Tracing crop-specific sediment sources in agricultural catchments. Geomorphology 139–140, 322–329.

Boix-Fayos, C., Nadeu, E., Quiñonero, J., Martínez-Mena, M., Almagro, M., De Vente, J., 2015. Sediment flow paths and associated organic carbon dynamics across a Mediterranean catchment. Hydrol. Earth Syst. Sci. 19, 1209.

Brindley, G.W., Brown, G. (Eds.), 1982. Crystal Structures of Clay Minerals and their X-ray Identification, 5. The Mineralogical Society of Great Britain and Ireland, London.

Cailleaud, E., 2015. Cycles du Carbone et de l'azote et Émissions de gaz à Effet de Serre (CH_4, CO_2 et N_2O) au lac de Barrage de Petit Saut et du Fleuve Sinnamary en Aval du Barrage (Guyane Française). Université de Toulouse, p. 258.

Caitcheon, G.G., 1993. Sediment source tracing using environmental magnetism - a new approach with examples from Australia. Hydrol. Process. 7, 349–358.

Chaplot, V., Poesen, J., 2012. Sediment, soil organic carbon and runoff delivery at various spatial scales. Catena 88, 46–56.

Chartin, C., Evrard, O., Laceby, J.P., Onda, Y., Ottlé, C., Lefèvre, I., Cerdan, O., 2017. The impact of typhoons on sediment connectivity: lessons learnt from contaminated coastal catchments of the Fukushima Prefecture (Japan). Earth Surf. Process. Landf. 42, 306–317.

Chartin, C., Evrard, O., Onda, Y., Patin, J., Lefèvre, I., Ottlé, C., Ayrault, S., Lepage, H., Bonté, P., 2013. Tracking the early dispersion of contaminated sediment along rivers draining the Fukushima radioactive pollution plume. Anthropocene 1, 23–34.

Chen, F., Fang, N., Wang, Y., Tong, L., Shi, Z., 2017. Biomarkers in sedimentary sequences: indicators to track sediment sources over decadal timescales. Geomorphology 278, 1–11.

Colombo, J., Silverberg, N., Gearing, J., 1997. Lipid biogeochemistry in the Laurentian trough—II. Changes in composition of fatty acids, sterols and aliphatic hydrocarbons during early diagenesis. Org. Geochem. 26, 257–274.

Coplen, T.B., Kendall, C., Hopple, J., 1983. Comparison of stable isotope reference samples. Nature 302, 236–238.

diCenzo, P.D., Luk, S.-H., 1997. Gully erosion and sediment transport in a small subtropical catchment, South China. Catena 29, 161–176.

Emerson, S., 1985. Organic carbon preservation in marine sediments. In: Sundquist, E.T., Broecker, W.S. (Eds.), The Carbon Cycle and Atmospheric CO: Natural Variations Archean to Present. American Geophysical Union, Washington, D.C., pp. 78–87.

Evrard, O., Chartin, C., Onda, Y., Lepage, H., Cerdan, O., Lefèvre, I., Ayrault, S., 2014. Renewed soil erosion and remobilisation of radioactive sediment in Fukushima coastal rivers after the 2013 typhoons. Sci Rep 4, 1–5.

Evrard, O., Laceby, J.P., Huon, S., Lefèvre, I., Sengtaheuanghoung, O., Ribolzi, O., 2016. Combining multiple fallout radionuclides (^{137}Cs, ^7Be, $^{210}Pb_{xs}$) to investigate temporal sediment source dynamics in tropical, ephemeral riverine systems. J. Soils Sediments 16, 1130–1144.

Evrard, O., Laceby, J.P., Lepage, H., Onda, Y., Cerdan, O., Ayrault, S., 2015. Radiocesium transfer from hillslopes to the Pacific Ocean after the Fukushima nuclear power plant accident: a review. J. Environ. Radioact. 148, 92–110.

Evrard, O., Laceby, J.P., Onda, Y., Wakiyama, Y., Jaegler, H., Lefèvre, I., 2016. Quantifying the dilution of the radiocesium contamination in Fukushima coastal river sediment (2011–2015). Sci Rep 6, 1–8.

Foucher, A., Laceby, J.P., Salvador-Blanes, S., Evrard, O., Le Gall, M., Lefèvre, I., Cerdan, O., Rajkumar, V., Desmet, M., 2015. Quantifying the dominant sources of sediment in a drained lowland agricultural catchment: the application of a thorium-based particle size correction in sediment fingerprinting. Geomorphology 250, 271–281.

Fox, J.F., Papanicolaou, A.N., 2007. The use of carbon and nitrogen isotopes to study watershed erosion processes. J. Am. Water Resour. Assoc. 43, 1047–1064.

Fry, B., 2006. Stable Isotope Ecology. Springer, New York, p. 308.

Fukushima, T., Arai, H., 2014. Radiocesium contamination of lake sediments and fish following the Fukushima nuclear accident and their partition coefficient. Inland Waters 4, 204–214.

Garcia-Sanchez, L., 2008. Watershed wash-off of atmospherically deposited radionuclides: review of the fluxes and their evolution with time. J. Environ. Radioact. 99, 563–573.

Garcia-Sanchez, L., Konoplev, A., 2009. Watershed wash-off of atmospherically deposited radionuclides: a review of normalized entrainment coefficients. J. Environ. Radioact. 100, 774–778.

Girardin, C., Mariotti, A., 1991. Analyse isotopique du ^{13}C en abondance naturelle dans le carbone organique: un système automatique avec robot préparateur. Cah ORSTOM Ser Pedologie 26, 371–380.

Giri, S.J., Diefendorf, A.F., Lowell, T.V., 2015. Origin and sedimentary fate of plant-derived terpenoids in a small river catchment and implications for terpenoids as quantitative paleovegetation proxies. Org. Geochem. 82, 22–32.

Gourdin, E., Huon, S., Evrard, O., Ribolzi, O., Bariac, T., Sengtaheuanghoung, O., Ayrault, S., 2015. Sources and export of particle-borne organic matter during a monsoon flood in a catchment of northern Laos. Biogeosciences 12, 1073–1089.

Grimshaw, D.L., Lewin, J., 1980. Source identification for suspended sediments. J. Hydrol. 47, 151–162.

GSJ, 2010. (Geological Survey of Japan). Seamless Digital Geological Map of Japan 1: 200,000. Research Information Database DB084, Geological Survey of Japan. National Institute of Advanced Industrial Science and Technology, Japan.

Haddadchi, A., Olley, J., Laceby, J.P., 2014. Accuracy of mixing models in predicting sediment source contributions. Sci. Total Environ. 497–498, 139–152.

He, Q., Walling, D.E., 1996. Interpreting particle size effects in the adsorption of ^{137}Cs and unsupported ^{210}Pb by mineral soils and sediments. J. Environ. Radioact. 30, 117–137.

Hedges, J.I., Oades, J.M., 1997. Comparative organic geochemistries of soils and marine sediments. Org. Geochem. 27, 319–361.

Hilton, R.G., Galy, A., Hovius, N., Horng, M.-J., Chen, H., 2010. The isotopic composition of particulate organic carbon in mountain rivers of Taiwan. Geochim. Cosmochim. Acta 74, 3164–3181.

Huon, S., Bellanger, B., Bonté, P., Sogon, S., Podwojewski, P., Girardin, C., Valentin, C., De Rouw, H., Velasquez, F., Bricquet, J.-P., Mariotti, A., 2006. Monitoring soil organic carbon erosion with isotopic tracers: two case studies on cultivated tropical catchments with steep slopes (Laos, Venezuela). In: E., R., R., L., B., B., C., F., B.A., S. (Eds.), Soil Erosion and Carbon Dynamics. Advances in Soil Science. CRC Press, Boca Raton, Florida, pp. 301–328.

Juracek, K.E., Ziegler, A.C., 2009. Estimation of sediment sources using selected chemical tracers in the Perry lake basin, Kansas, USA. Int. J. Sediment Res. 24, 108–125.

Kirkby, C., Kirkegaard, J., Richardson, A., Wade, L., Blanchard, C., Batten, G., 2011. Stable soil organic matter: a comparison of C:N:P:S ratios in Australian and other world soils. Geoderma 163, 197–208.

Knoll, L., Hagenbuch, E., Stevens, M., Vanni, M., Renwick, W., Denlinger, J.C., Hale, R.S., González, M., 2015. Predicting eutrophication status in reservoirs at large spatial scales using landscape and morphometric variables. Inland Waters 5, 203–214.

Koiter, A.J., Owens, P.N., Petticrew, E.L., Lobb, D.A., 2013. The behavioural characteristics of sediment properties and their implications for sediment fingerprinting as an approach for identifying sediment sources in river basins. Earth Sci. Rev. 125, 24–42.

Kurikami, H., Kitamura, A., Yamaguchi, M., Onishi, Y., 2013. Preliminary calculation of sediment and ^{137}Cs transport in the Ukedo River of Fukushima. Trans. Am. Nucl. Soc. 109, 149–152.

Kurikami, H., Kitamura, A., Yokuda, S.T., Onishi, Y., 2014. Sediment and ^{137}Cs behaviors in the Ogaki Dam Reservoir during a heavy rainfall event. J. Environ. Radioact. 137, 10–17.

Laceby, J.P., Chartin, C., Evrard, O., Onda, Y., Garcia-Sanchez, L., Cerdan, O., 2016. Rainfall erosivity in catchments contaminated with fallout from the Fukushima Daiichi nuclear power plant accident. Hydrol. Earth Syst. Sci. 20, 2467–2482.

Laceby, J.P., Evrard, O., Smith, H., Blake, W., Olley, J., Minella, J.P.G., Owens, P.N., 2017. The challenges and opportunities of addressing particle size effects in sediment source fingerprinting: a review. Earth Sci. Rev. 169, 85–103.

Laceby, J.P., Huon, S., Onda, Y., Evrard, O., 2016. Do forests represent a long-term source of contaminated particulate matter in the Fukushima prefecture? J. Environ. Manag. 183, 742–753.

Laceby, J.P., McMahon, J., Evrard, O., Olley, J., 2015. A comparison of geological and statistical approaches to element selection for sediment fingerprinting. J. Soils Sediments 15, 2117–2131.

Laceby, J.P., Olley, J., 2015. An examination of geochemical modelling approaches to tracing sediment sources incorporating distribution mixing and elemental correlations. Hydrol. Process. 29, 1669–1685.

Laceby, J.P., Olley, J., Pietsch, T.J., Sheldon, F., Bunn, S.E., 2015. Identifying subsoil sediment sources with carbon and nitrogen stable isotope ratios. Hydrol. Process. 29, 1956–1971.

Le Gall, M., Evrard, O., Foucher, A., Laceby, J.P., Salvador-Blanes, S., Thil, F., Dapoigny, A., Lefèvre, I., Cerdan, O., Ayrault, S., 2016. Quantifying sediment sources in a lowland agricultural catchment pond using ^{137}Cs activities and radiogenic ^{87}Sr/^{86}Sr ratios. Sci. Total Environ. 566–567, 968–980.

Lee, J., Yoshioka, T., Ra, K., Owen, J., Kim, B., 2011. Stable carbon and nitrogen isotope composition of co-existing herbivorous zooplankton species in an oligo-dystrophic lake (Shirakoma-ike, Japan). N. Z. J. Mar. Freshw. Res. 45, 29–41.

Legout, C., Poulenard, J., Nemery, J., Navratil, O., Grangeon, T., Evrard, O., Esteves, M., 2013. Quantifying suspended sediment sources during runoff events in headwater catchments using spectrocolorimetry. J. Soils Sediments 13, 1478–1492.

Lehmann, M.F., Bernasconi, S.M., McKenzie, J.A., Barbieri, A., Simona, M., Veronesi, M., 2004. Seasonal variation of the delta C-13 and delta N-15 of particulate and dissolved carbon and nitrogen in Lake Lugano: constraints on biogeochemical cycling in a eutrophic lake. Limnol. Oceanogr. 49, 415–429.

Lepage, H., Evrard, O., Onda, Y., Lefèvre, I., Laceby, J.P., Ayrault, S., 2015. Depth distribution of cesium-137 in paddy fields across the Fukushima pollution plume in 2013. J. Environ. Radioact. 147, 157–164.

Lepage, H., Laceby, J.P., Bonté, P., Joron, J.L., Onda, Y., Lefèvre, I., Ayrault, S., Evrard, O., 2016. Investigating the source of radiocesium contaminated sediment in two Fukushima coastal catchments with sediment tracing techniques. Anthropocene 13, 57–68.

Mariotti, A., Peterschmitt, E., 1994. Forest savanna ecotone dynamics in India as revealed by carbon isotope ratios of soil organic matter. Oecologia 97, 475–480.

Martinez-Carreras, N., Udelhoven, T., Krein, A., Gallart, F., Iffly, J.F., Ziebel, J., Hoffmann, L., Pfister, L., Walling, D.E., 2010. The use of sediment colour measured by diffuse reflectance spectrometry to determine sediment sources: application to the Attert River catchment (Luxembourg). J. Hydrol. 382, 49–63.

Matsuda, K., Takagi, K., Tomiya, A., Enomoto, M., Tsuboi, J.-I., Kaeriyama, H., Ambe, D., Fujimoto, K., Ono, T., Uchida, K., 2015. Comparison of the radioactive cesium contamination level of fish and their habitat among three lakes in Fukushima Prefecture, Japan, after the Fukushima fallout. In: Nakata, K., Sugisaka, H. (Eds.), Impacts of the Fukushima Nuclear Accident on Fish and Fishing Grounds. Springer, Tokyo, pp. 187–199.

McConnachie, J.L., Petticrew, E.L., 2006. Tracing organic matter sources in riverine suspended sediment: implications for fine sediment transfers. Geomorphology 79, 13–26.

Meyers, P.A., 1994. Preservation of elemental and isotopic source identification of sedimentary organic matter. Chem. Geol. 114, 289–302.

Mook, W., Tan, F., 1991. Stable carbon isotopes in rivers and estuaries. In: Degens, E.T., Kempe, S., Richey, J.E. (Eds.), Biogeochemistry of Major World Rivers. John Wiley & Sons, New Jersey, pp. 245–264.

Mouri, G., Golosov, V., Shiiba, M., Hori, T., 2014. Assessment of the caesium-137 flux adsorbed to suspended sediment in a reservoir in the contaminated Fukushima region in Japan. Environ. Pollut. 187, 31–41.

Murray, A.S., Olive, L.J., Olley, J.M., Caitcheon, G.G., Wasson, R.J., Wallbrink, P.J., 1993. Tracing the source of suspended sediment in the Murrumbidgee River, Australia. In: Peters, N.E., Hoehn, E., Leibundgut, C., Tase, N., Walling, D.E. (Eds.), Tracers in Hydrology, IAHS Publication No. 215. IAHS Press, Wallingford, pp. 293–302.

Nagao, S., Kanamori, M., Ochiai, S., Tomihara, S., Fukushi, K., Yamamoto, M., 2013. Export of ^{134}Cs and ^{137}Cs in the Fukushima river systems at heavy rains by Typhoon Roke in September 2011. Biogeosciences 10, 6215–6223.

Natelhoffer, K.J., Fry, B., 1988. Controls on natural nitrogen-15 and carbon-13 abundances in forest soil organic matter. Soil Sci. Soc. Am. J. 52, 1633–1640.

Naulier, M., Eyrolle-Boyer, F., Boyer, P., Métivier, J.-M, Onda, Y., 2017. Particulate organic matter in rivers of Fukushima: an unexpected carrier phase for radiocesiums. Sci. Total Environ. 579, 1560–1571.

Nguyen Tu, T.T.N., Egasse, C., Anquetil, C., Zanetti, F., Zeller, B., Huon, S., Derenne, S., 2017. Leaf lipid degradation in soils and surface sediments: a litterbag experiment. Org. Geochem. 104, 35–41.

Nieder, R., Benbi, D.K., Scherer, H.W., 2011. Fixation and defixation of ammonium in soils: a review. Biol. Fertil. Soils 47, 1–14.

NLA, 1972. (National Land Agency, Japan) Tochi-Bunrui-Zu Fukushima-ken (Land Classification Map for Fukushima Prefecture). Japan Map Center.

Onstad, G.D., Canfield, D.E., Quay, P.D., Hedges, J.I., 2000. Sources of particulate organic matter in rivers from the continental USA: lignin phenol and stable carbon isotope compositions. Geochim. Cosmochim. Acta 64, 3539–3546.

Owens, P.N., Blake, W.H., Gaspar, L., Gateuille, D., Koiter, A.J., Lobb, D.A., Petticrew, E.L., Raiffarth, D., Smith, H.G., Woodward, J.C., 2016. Fingerprinting and tracing the sources of soils and sediments: earth and ocean science, geoarchaeological, forensic, and human health applications. Earth Sci. Rev. 162, 1–23.

Owens, P.N., Blake, W.H., Petticrew, E.L., 2006. In: Kronvang, B., Faganeli, J., Ogrinc, N. (Eds.), Changes in sediment sources following wildfire in mountainous terrain: a paired-catchment approach, British Columbia, Canada. The Interactions Between Sediments and Water, Springer Netherlands, pp. 273–281.

Reiffarth, D., Petticrew, E., Owens, P., Lobb, D., 2016. Sources of variability in fatty acid (FA) biomarkers in the application of compound-specific stable isotopes (CSSIs) to soil and sediment fingerprinting and tracing: a review. Sci. Total Environ. 565, 8–27.

Remusat, L., Hatton, P.-J., Nico, P.S., Zeller, B., Kleber, M., Derrien, D., 2012. NanoSIMS study of organic matter associated with soil aggregates: advantages, limitations, and combination with STXM. Environ. Sci. Technol. 46, 3943–3949.

Rontani, J.-F., Volkman, J.K., 2003. Phytol degradation products as biogeochemical tracers in aquatic environments. Org. Geochem. 34, 1–35.

Saito, T., Makino, H., Tanaka, S., 2014. Geochemical and grain-size distribution of radioactive and stable cesium in Fukushima soils: implications for their long-term behavior. J. Environ. Radioact. 138, 11–18.

Sakaguchi, A., Tanaka, K., Iwatani, H., Chiga, H., Fan, Q., Onda, Y., Takahashi, Y., 2015. Size distribution studies of ^{137}Cs in river water in the Abukuma riverine system following the Fukushima Dai-ichi nuclear power plant accident. J. Environ. Radioact. 139, 379–389.

Sakai, Y., Karube, Z.i., Takeyama, T., Kohzu, A., Yoshimizu, C., Nagata, T., Tayasu, I., Okuda, N., 2013. Seasonal and site-specific variability in terrigenous particulate organic carbon concentration in near-shore waters of Lake Biwa, Japan. Limnology 14, 167–177.

Schimel, D.S., 1993. Theory and Application of Tracers. Isotopic Techniques in Plant, Soil and Aquatic Biology. Academic Press, Inc., San Diego, p. 119.

Schubert, C.J., Calvert, S.E., 2001. Nitrogen and carbon isotopic composition of marine and terrestrial organic matter in Arctic Ocean sediments: implications for nutrient utilization and organic matter composition. Deep-Sea Res. I Oceanogr. Res. Pap. 48, 789–810.

Smith, J.C., Galy, A., Hovius, N., Tye, A.M., Turowski, J.M., Schleppi, P., 2013. Runoff-driven export of particulate organic carbon from soil in temperate forested uplands. Earth Planet. Sci. Lett. 365, 198–208.

Sobek, S., Durisch-Kaiser, E., Zurbrügg, R., Wongfun, N., Wessels, M., Pasche, N., Wehrli, B., 2009. Organic carbon burial efficiency in lake sediments controlled by oxygen exposure time and sediment source. Limnol. Oceanogr. 54, 2243.

Thothong, W., Huon, S., Janeau, J.-L., Boonsaner, A., De Rouw, A., Planchon, O., Bardoux, G., Parkpian, P., 2011. Impact of land use change and rainfall on sediment and carbon accumulation in a water reservoir of North Thailand. Agric. Ecosyst. Environ. 140, 521–533.

Ueda, S., Hasegawa, H., Kakiuchi, H., Akata, N., Ohtsuka, Y., Hisamatsu, S.i., 2013. Fluvial discharges of radiocaesium from watersheds contaminated by the Fukushima Dai-ichi nuclear power plant accident, Japan. J. Environ. Radioact. 118, 96–104.

UNESCO, 1974. (United Nations Educational, Scientific and Cultural Organization). FAO/UNESCO Soil Map of the World. 1:5,000,000. UNESCO, Paris.

Walling, D.E., 2005. Tracing suspended sediment sources in catchments and river systems. Sci. Total Environ. 344, 159–184.

Walling, D.E., Kane, P., 1984. Suspended sediment properties and their geomorphological significance. In: Burt, T.P., Walling, D.E. (Eds.), Catchment Experiments in Fluvial Geomorphology. Geo Books, Norwich, pp. 311–334.

Walling, D.E., Woodward, J.C., 1995. Tracing sources of suspended sediment in river basins - a case-study of the River Culm, Devon, UK. Mar. Freshw. Res. 46, 327–336.

Wetzel, R.G., 2001. Limnology: Lake and River Ecosystems. Third Edition. Academic Press, San Diego, p. 1006.

Wilkinson, S., Olley, J., Furuichi, T., Burton, J., Kinsey-Henderson, A., 2015. Sediment source tracing with stratified sampling and weightings based on spatial gradients in soil erosion. J. Soils Sediments 15, 2038–2051.

Yamada, S., Kitamura, A., Kurikami, H., Yamaguchi, M., Malins, A., Machida, M., 2015. Sediment and ^{137}Cs transport and accumulation in the Ogaki dam of eastern Fukushima. Environ. Res. Lett. 10, 1–9.

Yamashiki, Y., Onda, Y., Smith, H.G., Blake, W.H., Wakahara, T., Igarashi, Y., Matsuura, Y., Yoshimura, K., 2014. Initial flux of sediment-associated radiocesium to the ocean from the largest river impacted by Fukushima Daiichi nuclear power plant. Sci Rep 4, 1–7.

Yasutaka, T., Naito, W., 2016. Assessing cost and effectiveness of radiation decontamination in Fukushima Prefecture, Japan. J. Environ. Radioact. 151, 512–520.

Yoshimura, K., Onda, Y., Fukushima, T., 2014. Sediment particle size and initial radiocesium accumulation in ponds following the Fukushima DNPP accident. Sci Rep 4, 1–6.

Yoshimura, K., Onda, Y., Wakahara, T., 2016. Time dependence of the ^{137}Cs concentration in particles discharged from rice paddies to freshwater bodies after the Fukushima Daiichi NPP accident. Environ. Sci. Technol. 50, 4186–4193.